

Numerical Study on Debonding Failure between FRP and Concrete

†Lihua Huang¹; Zhiquan Yang¹; and Yuefang Wang²

¹School of Civil Engineering, Dalian University of Technology, China.

²Department of Engineering Mechanics, Dalian University of Technology, China.

*Presenting author: lhhang@dlut.edu.cn

†Corresponding author: lhhang@dlut.edu.cn

Abstract

Fiber reinforced polymer (FRP) has been widely employed in retrofitting concrete structures. Debonding of FRP from concrete is a typical failure mode in this technique. Cohesive zone model (CZM) of fracture energy-based criteria is demonstrated to be a well-founded numerical approach to characterize the brittle behavior of interfacial debonding failure. A simple but robust finite-element (FE) model of CZM for simulating the debonding procedure induced by the intermediate concrete crack (IC) and discontinuous FRP edge is presented in this paper. The bilinear bond-slip relationship in the interface is applied in the numerical model. Ten FRP strengthened beams of IC debonding and edge debonding failures are simulated by the suggested FE model and verified by the experimental results. For FRP strengthened plain concrete beams of pre-cracks, the variations of applied loads with concrete crack mouth open displacements (CMOD) can be accurately revealed, and when the cohesive strength in the interfacial bilinear model is reduced to 40%, the edge debonding failures of reinforced concrete beams can be accurately illustrated. The variations of stress and strain in FRP and concrete as well as in the interface with the increase of CMODs and deflections are expediently and expressly indicated through the proposed FE model.

Keywords: **FRP; Concrete beam; CZM; IC debonding, Edge debonding**

Introduction

External bonding of fiber reinforced polymer (FRP) sheet or plate has been widely accepted as an effective and convenient technique for the strengthening of concrete structures. One of the key factors that influence the strengthening is the interfacial debonding failure of FRP from substrate [1]-[4]. The behavior of FRP-to-concrete interfaces has been deeply investigated, and well expressed by bond-slip models [5][6], which make the prediction of interfacial debonding possible. Among the debonding failure modes, one is caused by the opening up of concrete flexural cracks and the debonding initiates from those places. This kind of debonding failure is commonly referred to as the intermediate concrete crack (IC)-induced debonding [7]. Another main failure mode is named as the edge debonding because the interfacial debonding initiates from the edge of FRP sheet and then propagates towards the middle of the interface.

The sound analytical studies on interfacial debonding have been conducted by many researchers, where the self-programming finite element (FE) models are developed to predict the load-deflection behavior. Although the proposed models are demonstrated to be valid, most of them are lack of accessibility. The primitive versatile numerical models are commonly based on the strength of interfacial shear stress represented by the bridging elements such as link and spring [8]-[10], which is actually inconsistent with the interfacial brittleness of debonding process. Fracture energy approach is recognized to be more appropriate to capture the interfacial fracture behavior and account for the possible failure

modes [6]. Among the FE models of fracture energy-based criteria, cohesive zone modeling(CZM) approach is well known for its simplicity and accurate kinematics representation of the quasi-brittle fracture process zone, which arises prior to complete fracture in, e.g., concrete materials and macro-molecular based polymer materials[11][12]. The bond-slipping of the interface can be governed by a fundamental fracture energy that is also the energy required to break apart the interface surfaces in this model. The whole debonding process from crack initiation to growth and further slipping can be unified into one model and easily formulated and implemented by CZM. According to this idea, Wang(2006) has established the closed-form solution of CZM for IC induced debonding[13]. De Lorenzis(2009) and Cornetti(2015) put forward an analytical cohesive crack modeling approach to the edge debonding failure of FRP-plated beam[14] [15]. Chen(2009) conducted debonding analysis of adhesively bonded interface between two balanced adjacent flexural cracks by CZM[16]. As stressed in many studies, much further research is needed to develop a simple and accurate simulating model that has a rational theoretical basis and a practical engineering application.

In the present work, the most common debonding failures of FRP strengthened concrete beams are simulated by applying the proposed FE model of CZM based on the FE package ABAUSE/standard. Two rational models are developed to easily reveal the processes of IC-induced debonding and FRP edge debonding. Exponential degradation of concrete cracking and bilinear relationship between interfacial shear stresses and slips proposed by Lu(2005) are assigned as to the properties of the interfaces[5]. To demonstrate the validity of the numerical models, the corresponding experimental data from the literatures are taken as the verification of the numerical results. As the governing parameters in CZM, the values of the maximum interfacial shear stress and the fracture energy have been discussed. The simple FEM and suggested parameters are provided to be useful for predicting the propagation of debonding failures between FRP/concrete interfaces.

Material Modeling

Concrete, Steel and FRP Composite

The reduction of the strength and stiffness of concrete is represented by the plastic-damage model introduced in ABAQUS. The uniaxial compressive stress-strain curve for concrete is determined by the equation of Hognestad[17][18], in which the maximum strain is taken as $\epsilon_{cu} = 0.0038$. For the finite-element implementation, the values of the tensile strength, f_t , and elastic modulus, E_0 , if not given, are approximated based on the following ACI-318-05[19] equations:

$$E_0 = 4730\sqrt{f_c'} \quad (1)$$

$$f_t = 0.53\sqrt{f_c'} \quad (2)$$

Concrete is assumed to be elastic before cracking. The tensile degradation of concrete is expressed by the exponential equation of Reinhardt [18][20] in fracture mechanics as follow:

$$\frac{\sigma_t}{f_t} = \left[1 + \left(\frac{c_1 \omega}{\omega_0} \right)^3 \right] \exp\left(-\frac{c_2 \omega}{\omega_0}\right) - \frac{\omega}{\omega_0} (1 + c_1^3) \exp(-c_2) \quad (3)$$

where cohesive stress, σ_t , is corresponding to the open distance of crack, ω . Factors, $c_1=3$, $c_2=7$ for normal concrete. $\omega_0=0.16$ mm as $\sigma_t=0$.

Steel is represented by an elastic-plastic constitutive relationship with linear strain hardening, and FRP is assumed to be linear elastic constitutive relationship.

FRP/Concrete Interface

In the current study, the bilinear bond-slip model proposed by Lu(2005), as shown in figure 1, is adopted for its simplicity and easy incorporation into the FE analysis [5]. The behavior of the FRP/concrete interface is modified as a relationship between the local shear stress, τ , and the relative displacement, s , as follow.

$$\beta_\omega = \sqrt{\frac{2.25 - b_f / b_c}{1.25 + b_f / b_c}} \quad (4)$$

$$\tau_{\max} = 1.5\beta_\omega f_t \quad (5)$$

$$s_0 = 0.0195\beta_\omega f_t \quad (6)$$

$$G_f = 0.308\beta_\omega^2 \sqrt{f_t} \quad (7)$$

in which b_f / b_c and f_t are the ratio of the width of FRP to concrete and the splitting tension strength of concrete, respectively.

The maximum nominal stress criterion is applied to determine the initiation of interfacial cracking, namely shear crack develops at the point τ_{\max} . Interfacial performance of bond-slip is governed by the cohesive strength τ_{\max} and the fracture energy G_f , which are essentially identical in this model.

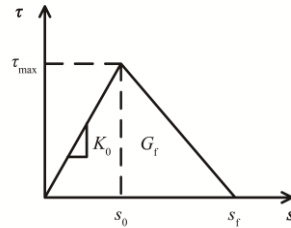


Figure 1. Bilinear bond-slip model

FE Modeling of IC Debonding

Profile of the Strengthened Beams with IC Debonding

IC debonding failure has been experimentally investigated by many researchers through testing FRP strengthened plain concrete beams of various seam-height ratios. Three-point bending beams of different heights, lengths, and seam height ratios from the literature[21] are simulated by using the FE model of CZM in this paper. FRP is of the same length, but one-third width of concrete beam. To prevent the conical shear failure around intermediate crack, unbonded segment is set up near the crack.

Parameters such as the splitting tension strength of concrete, the flexural strengths of beams with different heights, tensile strength of CFRP, modulus of elasticity and Poisson's ratios of concrete and CFRP are taken from the experimental data in the literature[21].

Based on the experimental data, the maximum shear stress and the fracture energy are determined according to the equations (4)-(7), namely $\tau_{\max}=5.94$ MPa, $G_f=0.7$ N/mm, and the maximum slip $s_f=2G_f / \tau_{\max} = 0.236$ mm as the interfacial debonding occurs.

Constitutive Properties of Concrete Cracking

Since IC debonding is induced by the propagation of intermediate concrete crack, the modeling of concrete cracking with CZM is essentially identified first. It is assumed that concrete is a linearly elastic material when the equivalent stress in plain concrete is less than $0.3f_c$ [22]. Fictitious cracking model is adopted to avoid the singularity of crack tip in FEA. According to the exponential concrete virtual crack model proposed by Reinhardt[17][20], equivalent crack opening displacement $\omega_0=0.16\text{mm}$ when cohesive force decreases to zero. The maximum nominal stress criterion is applied for modeling the initiation of concrete crack, in which fictitious crack develops when tensile stress reaches to the flexural strength of concrete. Equations of cohesive force with crack opening distance is expressed by

$$f(\delta) = f_t \left[1 - \frac{1 - e^{-\alpha \left(\frac{\delta - \delta_0}{\delta_f - \delta_0} \right)}}{1 - e^{-\alpha}} \right] \quad (8)$$

$$\delta_0 = 1 \times \frac{f_t}{E_c} \quad (9)$$

where f_t is the flexural strength of concrete; default value is one for zero constitutive thickness of cohesive element; δ_f represents the open distance of crack when cohesive force equals zero, namely $\delta_f = \omega_0$. Coefficient, α , is used to govern the curves of exponential degradation of concrete, which is determined by the experimental data in literature [21]. When $\alpha=10$, as listed in table 1, the peak loads of five beams determined by numerical solution, P_{Num} , are close to the experimental values, P_{Exp} . Based on the equations (8), (9) and the parameter α , the constitutive relationships between loads and crack mouth open displacements (CMOD) of the concrete beams are constructed as shown in figure 2, which are also the curves for governing IC propagation.

Table 1. Comparison of numerical and experimental peak loads

Beams	P_{Exp}/kN	P_{Num}/kN	Error /%
C202	9.4	10.07	7.13
C203	6.93	8.08	16.60
C204	5.65	6.05	7.08
C253	8.69	9.42	8.40
C303	9.92	10.02	1.01

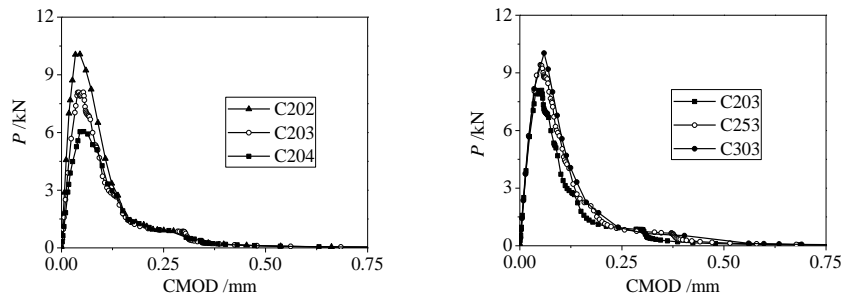


Figure 2. Curves of load-CMOD of the concrete beams

Numerical and Experimental Results Comparison

In the FE model, the concrete and the FRP are modeled by solid C3D8R and shell S4R in the package ABAQUS. The unbonded segment around intermediate crack is treated as frictionless contact. Cohesive elements COH3D8 are embedded in the middle of concrete beam and the FRP/concrete interface for identifying the IC propagation and FRP debonding. The five plain beams bonded with CFRP from literature[21] are simulated by the suggested FE model of CZM, and the corresponding load-CMOD curves are constructed, as shown in figure 3. It is shown that, close to the experimental results, there are apparently two peak points of loads, P_{1max} and P_{2max} . The applied load is linearly proportional to CMOD when it is less than P_{1max} . After the first peak point, the load decreases with the IC propagation. Then the load rises again until to the second peak point due to the activation of CFRP. Interfacial slip starts at this time. The numerical results obtained from the suggested FE model are well agreeable with the experimental results, as shown in table 2 and figure 3.

Table 2. Comparison of the peak loads obtained from the FEM and experiments

Beams	P_{1Num}/kN	P_{1Exp}/kN	Error/%	P_{2Num}/kN	P_{2Exp}/kN	Error/%
P202	11.30	10.97	3.00	11.98	11.95	0.25
P203	8.71	9.07	3.97	11.97	11.66	2.66
P204	6.73	7.72	12.82	11.97	12.33	2.92
P253	9.88	11.18	11.63	11.96	12.80	6.56
P303	10.34	12.93	20.03	12.02	13.55	11.29

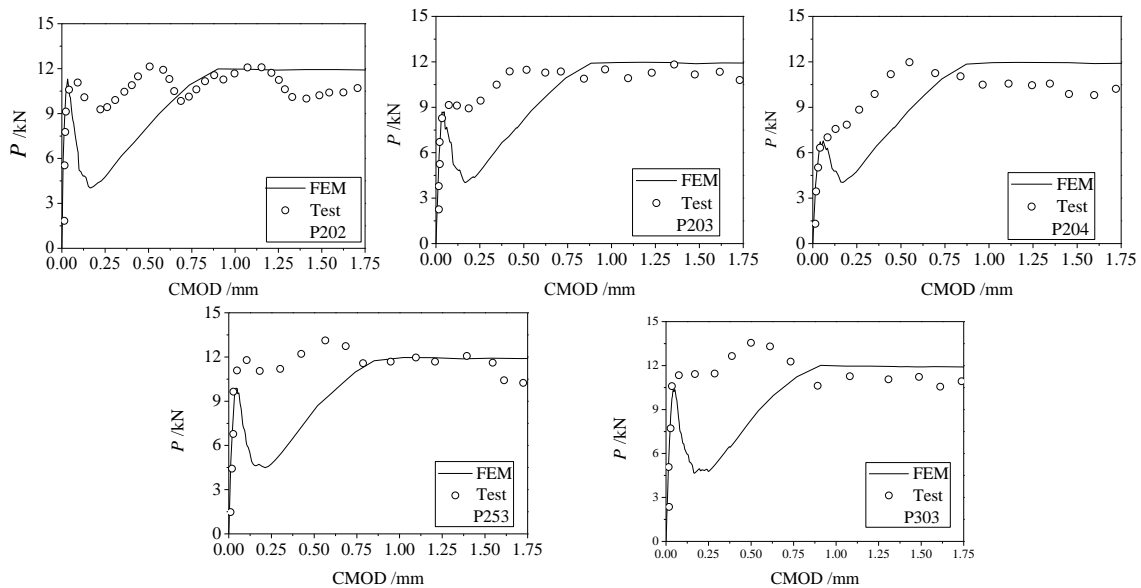


Figure 3. Comparison of load-CMOD curves obtained from the FEM and experiments

Identification of IC-induced Debonding

Stress distribution of CFRP of beam 203 under different CMOD is constructed in figure 4. It is shown that the stress at the middle of CFRP linearly increases with CMOD before the applied load reaches to P_{2max} . When the load equals to P_{1max} , where CMOD equals to 0.046 mm as shown in figure 4, stress in CFRP remains in a low level, namely 88MPa. While, when the applied load equals to P_{2max} , where CMOD equals to 1.183 mm, stress in CFRP reaches to

the highest value of 1430 MPa. Then the stresses remain in a high level with the continuous increase of CMOD, and gradually transfer from the middle to the edge of CFRP. It illustrates that the stress in CFRP is mainly caused by the IC propagation and interfacial slip. When CMOD reaches to 2.968 mm, most of the CFRP stays in a high stress level of 1430 MPa, as shown in figure 4.

Stresses in concrete indicate that most of the concrete stay in a low stress level because of concrete cracking and interfacial slipping. Stress concentrations are obvious at the tips of concrete crack and interfacial shear crack, and the maximum stress is close to the flexural strength of concrete. Cohesive stress distribution of concrete crack under specific CMOD is shown in figure 5. When the applied load reaches to P_{1max} , fictitious crack is of 55 mm length and the cohesive tensile stress near the tip of concrete crack is 0.870 MPa. As the load reaches to P_{2max} , the fictitious crack extends to 135 mm and the macro-crack to 105 mm at the same time. Because of the extension of concrete crack, the loading capacity of FRP-bonded concrete beam gradually decreases after the applied load exceeds P_{1max} , and most of the load is sustained by CFRP with little contribution of concrete after the applied load exceeds P_{2max} .

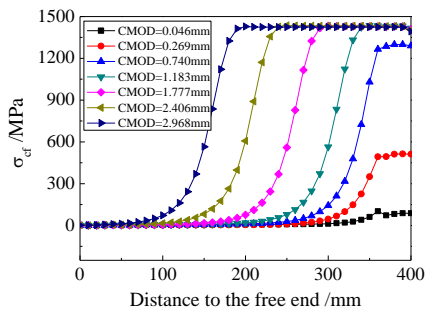


Figure 4. Stresses of CFRP

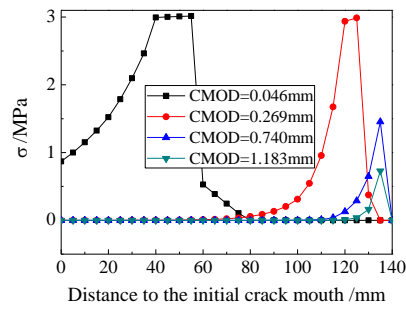


Figure 5. Adhesive stress of concrete crack

Along with the increase of CMOD, the interfacial bonding stress moves from the middle toward the edge, as shown in figure 6. When the applied load equals to P_{1max} , where CMOD equals 0.046mm, the maximum interfacial shear stress is 0.5MPa. Interface behaves in elastic with a low level of shear stress. Interfacial shear stress near the intermediate crack decreases to zero when the applied load increases to the second peak load P_{2max} , namely CMOD getting to 1.183 mm. Macro shear crack of 20mm length occurs at this time. The interfacial shear stress gradually moves from the middle to the edge due to the enlargement of CMOD.

Variation of interfacial slip with CMOD is plotted in figure 7. Analogous to the interfacial shear stress, interfacial slip extends from the middle to the edge of the interface following the enlargement of CMOD. The inflection points of the curves in figure 7 are corresponding to the maximum shear stresses presented in figure 6.

FE Modeling of Edge Debonding

Edge Debonding Failure in FRP Strengthened RC Beams

FRP strengthened RC beams of four-point bending are taken from the experiments in literature[23][24]. Five beams with the edge debonding are simulated by the proposed FE model of bilinear bond-slip interfacial property. Based on the experimental data, the maximum shear stress and the fracture energy are determined according to the equations (4)-(7), and the maximum slip $s_f = 2F_f / \tau_{max}$ as the interfacial debonding occurs.

Concrete, steel bar and CFRP are modeled with solid C3D8R, truss T3D2 and shell S4R in the package ABAQUS, respectively. Interfacial bond-slip is represented by COH3D8. Slipping between concrete and steel bars is neglected. The numerical load-displacement curves determined by the supposed FE model are compared with the experimental results, as shown in table 3. It is shown that the peak loads determined by the numerical model are well agreeable with the experimental results.

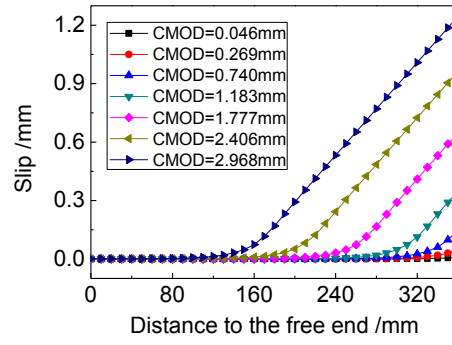
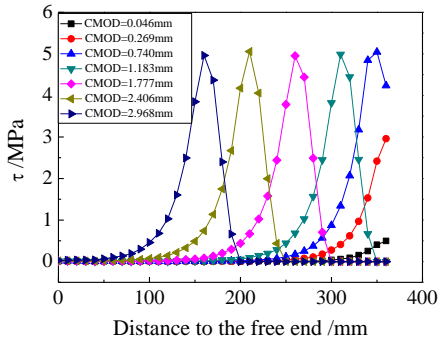


Figure 6. Variation of interfacial stress **Figure 7. Variation of interfacial slip**

Table 3. Numerical and experimental peak loads

Literature	Beams	P_{Num}/kN	P_{Exp}/kN	Error/%
Obaidat[23]	RF1	166.2	166	0.1
	RF2	146.5	142	3.2
	RF3	129.9	128	1.5
Quantrill[24]	B2	35.4	34	4.1
	B3	26.8	24.6	8.9

The numerical curves of load-displacement are compared with the experimental data, and plotted in Figure 8. It is shown that beams analyzed by the FE model exhibit greater ductility than the specimen. The deflections of the beams are bigger than the real beams when the applied loads reach or exceed the peak loads. The reasons that lead the exaggeration of ductility in FE analysis lie in that concrete is assumed to be an elastic-plastic property excluding the effect of concrete crack.

Parameters in Bond-slip Relationship

If the fracture energy G_f determined by equation (7) remains constant, and the maximum cohesive shear stress is assumed to be $0.3\tau_{max}$, $0.4\tau_{max}$, $0.5\tau_{max}$, $0.6\tau_{max}$ or $1.0\tau_{max}$, where τ_{max} is determined by equations (5), the curves of load-displacement from the FE model are constructed and compared with the experimental results, as shown in figure 9. Beam RF3 is not discussed since there is no obvious strengthening effect for short strengthening length. It can be seen that when the maximum shear stress is greater than $0.4\tau_{max}$, the values of the maximum shear stress have little effect on the peak loads, but greatly increase deflections. If the maximum shear stress is smaller than $0.3\tau_{max}$, the peak loads are apparently lower than the real values. The curves of load-displacement obtained from the FE model are the closest to the experimental results when the maximum interfacial shear stress equals to $0.4\tau_{max}$. There are apparent downward jumps to the loading strength of non-strengthened beams when

debonding occurs in the curves. The loading capacities of the strengthened beams are obviously controlled by the debonding of FRP, and the region of damage in the interface narrows down with the increase of the maximum shear stress. Therefore, the rational maximum shear stress in CZM is suggested to be $0.4\tau_{\max}$ in the FE analysis of FRP debonding from RC beams.

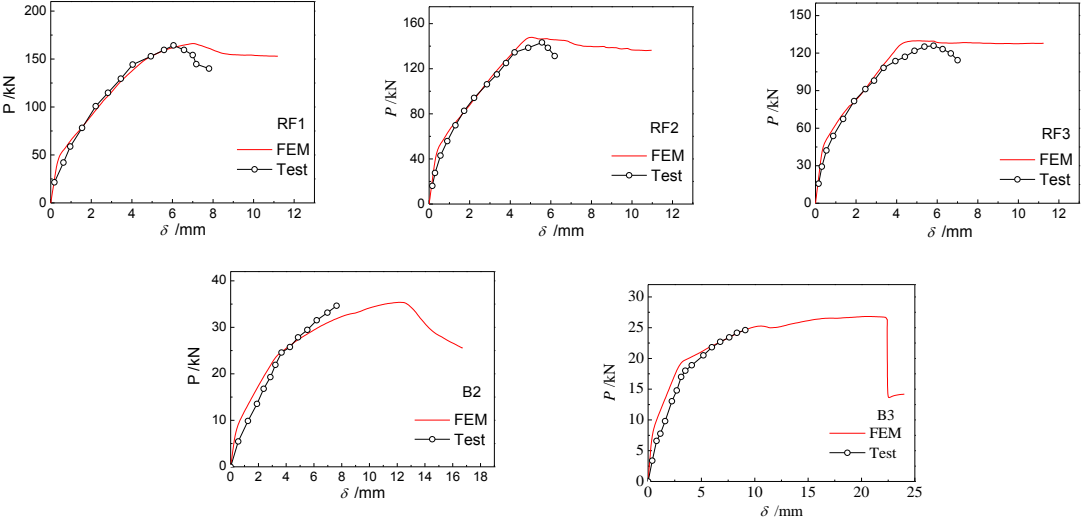


Figure 8. Load-displacement curves from FEM and experiments

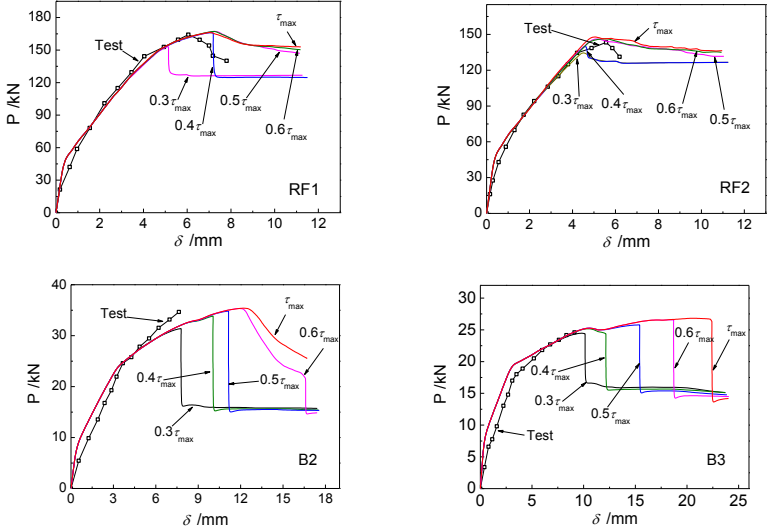


Figure 9. Load-displacement curves of different cohesive strength

The effect of fracture energy in CZM on numerical results is studied below. If the maximum shear stress is identified as $0.4\tau_{\max}$, and the fracture energy is taken as $0.5G_f$, $0.75G_f$, G_f , $1.25G_f$ or $1.5G_f$, where G_f is determined based on the equation (7), the corresponding load-displacement curves are constructed in figure 10. It can be seen that the ductility is exaggerated with the increase of the fracture energy. Large values of fracture energy result the failure of concrete crushing rather than FRP debonding as shown in the beams RF1 and RF2 in the case of fracture energy greater than $1.5G_f$. Small values of fracture energy result lower prediction of loading strength as shown in the curves of $0.5G_f$. The loading capacities of beams are obviously improved with the increase of fracture energy as it is less than G_f , and is

little upgraded when the fracture energy is greater than G_f . The curves of load-displacement are the closest to the experimental results when fracture energy equals to G_f .

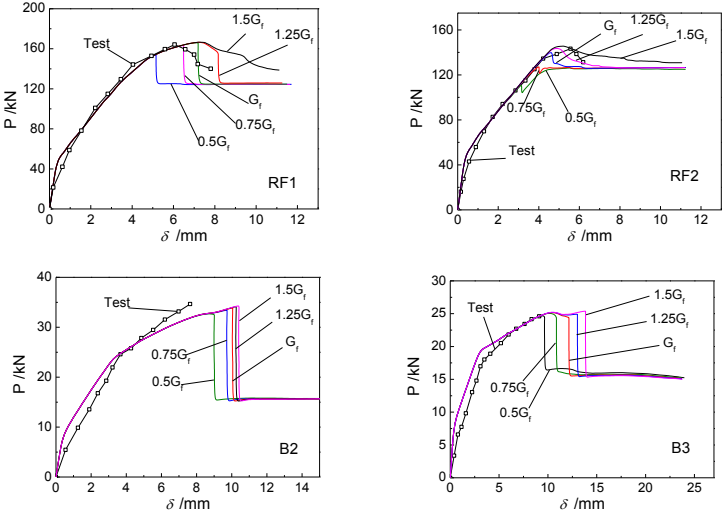


Figure 10. Influence of the fracture energy in CZM on FE analysis

Identification of Edge Debonding

Based on the forgoing discussion, the fracture energy determined by the equation (7) and the maximum shear stress modified to $0.4\tau_{max}$ are applied in the FEA of beam RF1. Stress distribution in FRP shows that the tensile stress at the edge of FRP reaches to the maximum, 35MPa, when the deflection at the middle of the beam reaches to 6.2mm. Later, the stress decreases quickly with the increase of deflection until to zero when deflection d equals 7.2mm, as shown in figure 11. Stress at the middle of FRP nonlinearly increases to 667MPa as $d=7.2$ mm, and then drops rapidly to a very low level due to the edge debonding, as illustrated in figure 12. The curves of stress distributions along FRP with respect to the enlargement of deflections clearly indicate that the stresses gradually increase with deflection until to the peak load, where $d=7.1$ mm, and then rapidly drops to very low level as $d=9$ mm shown in figure 13.

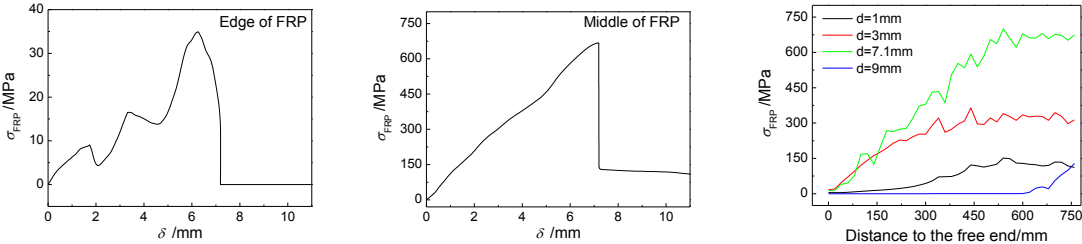


Figure 11. Stress at the edge Figure 12. Stress in the middle Figure 13. Stress along FRP

The behavior of interface between FRP and concrete is illustrated in figure 14-17. The stress at the edge of interface increases with deflection until to the maximum 3.5 MPa, where $d=3.4$ mm, and then gradually decreases to zero as deflection equals 7.2 mm in figure 14. At the middle of the interface in figure 15, the stress stays in a very low level about 1MPa before

edge debonding occurs. Then it rapidly increases to the maximum corresponding to the peak load at the moment of edge debonding. Afterward, stress stays in a very high level as debonding propagates from the edge to the middle of the beam. The distributions of stresses and slips along the interface under various deflections are shown in figure 16 and figure 17. Before the peak load, the interfacial stresses increase with the deflections, while slips stay in low levels. After the peak load, most of the interfacial stresses drop to zero and the slips greatly upgrade in the relevant region of the interface.

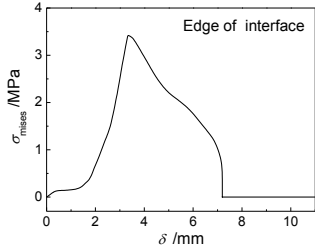


Figure 14. Stress at the edge of interface

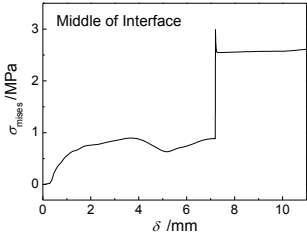


Figure 15. Stress at the middle of interface

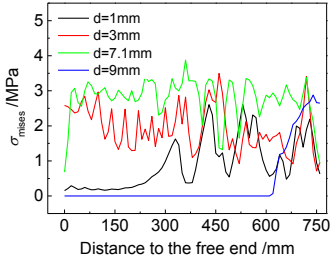


Figure 16. Interfacial stress distributions

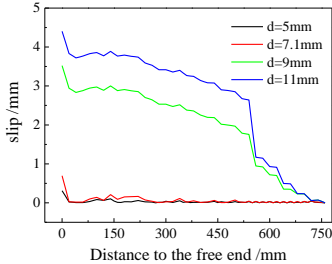


Figure 17. Interfacial slip distributions

The performance of concrete is revealed in figure 18 and figure 19. At the moment of the edge debonding, there is a downward jump in the curves of concrete stresses at the middle of the beam with respect to deflection. Afterwards, stresses continue to upgrade with the increase of deflection. When most of the FRP has debonded at the moment $d=11.5\text{mm}$, the stress and strain contours indicate that the biggest equivalent plastic strain occurs at the bottom of concrete, which is agreeable with the peeling of concrete surface happened in many experiments.

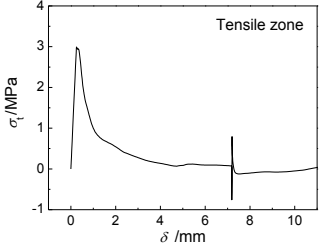
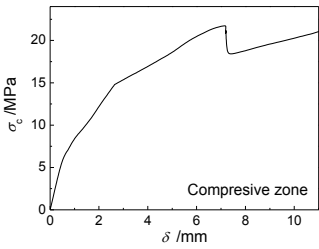


Figure 18. Curves of concrete stresses at the middle of beam to deflections

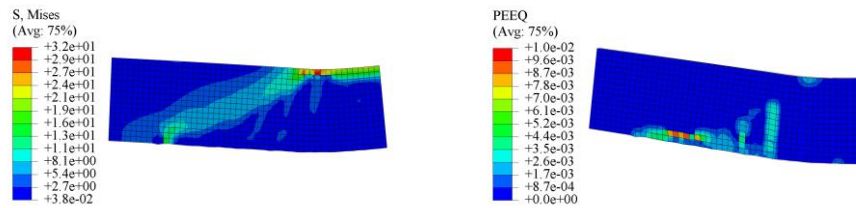


Figure 19. Stress and strain contour of concrete

Conclusions

A simple but robust FE model of fracture criteria-based CZM is set up for simulating the debonding failures of FRP strengthened concrete beams in this paper. Two types of debonding processes are analyzed: IC debonding and edge debonding. In the FEA of IC debonding, cohesive elements of concrete fracture properties are embedded in the middle of beam as to indicate the effects of flexural cracking on interfacial debonding. Cohesive elements in the interface between FRP and concrete are assigned bilinear bond-slip properties. The interfacial debonding failure revealed by the FE model is verified to be well consistent with the experimental phenomenon. When the suggested FE model is applied to simulate the edge debonding of FRP strengthened RC beam, parameters in CZM must be modified because concrete is assumed to be of elastic-plastic properties, which leads the exaggeration of the ductility when Lu's bond-slip relation is employed in the CZM. When the fracture energy and the maximum interfacial bonding stress are assigned G_f and $0.4\tau_{\max}$, the edge debonding process of FRP strengthened RC beam is reasonably predicted and well captured.

Acknowledgements

The research was funded by the Liaoning Science and Technology Project 2014020008.

References

- [1] Teng J. G., Chen J. F. (2008) Mechanics of debonding in FRP-plated RC beams, *Structures and Granular Solids: From Scientific Principles to Engineering Application*, 313.
- [2] Saxena P., Toutanji H., Noumowe A. (2008) Failure analysis of FRP-strengthened RC beams, *Journal of Composites for Construction*, **12**(1), 2–14.
- [3] Buyukozturk O., Gunes O., Karaca E. (2004) Progress on understanding debonding problems in reinforced concrete and steel members strengthened using FRP composites, *Construction and Building Materials*, **18**(1), 9–19.
- [4] Yao J., Teng J. G., Chen J. F. (2005) Experimental study on FRP-to-concrete bonded joints, *Composites Part B: Engineering*, **36**(2), 99–113.
- [5] Lu X. Z., Teng J. G., Ye L. P. (2005) Bond-slip models for FRP sheets/plates bonded to concrete, *Engineering Structures*, **27**(6), 920–937.
- [6] Toutanji H., Han M., Ghorbe El. (2012) Interfacial bond strength characteristics of FRP and RC substrate, *Journal of Composites for Construction*, **16**(1), 35–46.
- [7] Teng J. G., Smith S. T., Yao J. (2003) Intermediate crack-induced debonding in RC beams and slabs, *Construction and Building Materials*, **17**(6), 447–462.
- [8] Baky H. A., Ebead U. A., Neale K. W. (2007) Flexural and interfacial behavior of FRP-strengthened reinforced concrete beams, *Journal of Composites for Construction*, **11**(6), 629–639.
- [9] Lu X. Z., Ye L. P., Teng J. G. (2005) Meso-scale finite element model for FRP sheets/plates bonded to concrete, *Engineering Structures*, **27**(4), 564–575.
- [10] Lu X. Z., Teng J. G., Ye L. P., Jiang J. J. (2007) Intermediate crack debonding in FRP-strengthened RC beams: FE analysis and strength model, *Journal of Composites for Construction*, **11**(2), 161–74.
- [11] Xu R., Liu C. (2011) CZM-based debonding simulation of cracked beams strengthened by FRP sheets, *Journal of Engineering Mechanics*, **138**(2), 210–220.
- [12] Yang Q. D., Thouless M. D., Ward S. M. (1999) Numerical simulations of adhesively-bonded beams failing

- with extensive plastic deformation, *Journal of the Mechanics and Physics of Solids*, **47(6)**, 1337–1353.
- [13] Wang J. (2006) Cohesive zone model of intermediate crack-induced debonding of FRP-plated concrete beam, *International Journal of Solids and Structures*, **43(21)**, 6630–6648.
- [14] De Lorenzis L., Zavarise G. (2009) Cohesive zone modeling of interfacial stresses in plated beams, *International Journal of Solids and Structures*, **46(24)**, 4181–4191.
- [15] Cornetti P., Corrado M., De Lorenzis L. (2015) An analytical cohesive crack modeling approach to the edge debonding failure of FRP-plated beams, *International Journal of Solids and Structures*, **53**, 92–106.
- [16] Chen F., Qiao P. (2009) Debonding analysis of FRP–concrete interface between two balanced adjacent flexural cracks in plated beams, *International Journal of Solids and Structures*, **46(13)**, 2618–2628.
- [17] Reinhardt H. W., Cornelissen H. A. W., Hordijk D. A. (1986) Tensile tests and failure analysis of concrete, *Journal of Structural Engineering*, **112(11)**, 2462–2477.
- [18] Hillerborg A., Modér M., Petersson P. E. (1976) Analysis of crack formation and crack growth in concrete by means of fracture mechanics and finite elements, *Cement and Concrete Research*, **6(6)**, 773–781.
- [19] American Concrete Institute. (2004) *Building Code Requirements for Structural Concrete (ACI 318-05) and Commentary (ACI 318R-05)*, American Concrete Inst.
- [20] Reinhardt H. W., Cornelissen H. A. W., Hordijk D. A. (1986) Tensile tests and failure analysis of concrete, *Journal of Structural Engineering*, **112(11)**, 2462–2477.
- [21] Yi F. M. (2010) The fracture properties of CFRP strengthened Cracked concrete beam, *Doctoral Dissertation*, Dalian University of Technology.
- [22] Buyukozturk O. (1997) Nonlinear analysis of reinforced concrete structures, *Computers and Structures*, **7(1)**, 149–156.
- [23] Obaidat Y. T., Heyden S., Dahlblom O. (2011) Retrofitting of reinforced concrete beams using composite laminates, *Construction and Building Materials*, **25(2)**, 591–597.
- [24] Quantrill R. J., Hollaway L. C., Thorne A. M. (1996) Experimental and analytical investigation of FRP strengthened beam response: Part I, *Magazine of Concrete Research*, **48(177)**, 331–342.